Inorganic Chemistry
Article

Inorg. Chem. **2010**, *49*, 6725–6733 **6725**
DOI: 10.1021/ic100722w

Ga^{III} Complexes as Models for the M^{III} Site of Purple Acid Phosphatase: Ligand Effects on the Hydrolytic Reactivity Toward Bis(2,4-dinitrophenyl) phosphate

Fergal Coleman, Michael J. Hynes, and Andrea Erxleben*

School of Chemistry, National University of Ireland, Galway, Ireland

Received April 15, 2010

The effects of a series of Ga^{III} complexes with tripodal ligands on the hydrolysis rate of the activated phosphate diester bis(2,4-dinitrophenyl)phosphate (BDNPP) have been investigated. In particular, the influence of the nature of the ligand donor sites on the reactivity of Ga^{III} which represents a mimic of the Fe^{III} ion in purple acid phosphatase has been evaluated. It has been shown that replacing neutral nitrogen donor atoms and carboxylate groups by phenolate groups enhanced the reactivity of the Ga complexes. Bell-shaped pH-rate profiles and the measured solvent deuterium isotope effects are indicative of a mechanism that involves nucleophilic attack on the coordinated substrate by Ga−OH. The trend in reactivity found for the different Ga complexes reveals that of the two effects of the metal, Lewis acid activation of the substrate and nucleophile activation, the latter one is more important in determining the intrinsic reactivity of the metal catalyst. The relevance of the present findings for the modulation of the activity of the M^{III} ion in purple acid phosphatase whose active site contains a phenolate (tyrosine side chain) is discussed.

Introduction

Purple acid phosphatases (PAPs) are ubiquitous enzymes found in animals, plants, fungi, and bacteria. They contain a dinuclear $Fe^{III}M^{II}$ core, where M^{II} = Fe, Zn, or Mn, and catalyze the hydrolysis of a variety of phosphate ester substrates in the pH range 4−7.[1,2] Ga^{III} is an excellent mimic of Fe^{III} with similar ionic radius and Lewis acidity and can replace Fe^{III} in non-natural forms of PAP.[3,4] Crystal structures of red kidney bean,[5] rat,[6,7] pig,[8] human,[9] and sweet potato[10] PAP have been published. The metal ions were found to be coordinated by seven invariant amino acid side chains: In the resting state, Fe^{III} is bound by a tyrosine, a histidine, and an aspartate residue, while the M^{II} ion is surrounded by an asparagine and two histidine residues. A bridging monodentate carboxylate group of an aspartate side chain, a modeled bridging μ-OH group, and a modeled terminal water ligand complete the coordination spheres of the five- and six-coordinate Fe^{III} and M^{II} ions. The conserved tyrosine ligand of Fe^{III} is responsible for the characteristic purple color of the enzyme (phenolate-to-Fe^{III} charge-transfer at about 560 nm) and probably stabilizes the +III oxidation state of the Fe.[1−3] Despite the availability of detailed structural data, the catalytic mechanism of PAP is not fully understood to date. The substrate coordination mode as well as the identity of the attacking nucleophile remain a matter of debate, and two different mechanisms have been proposed.[1,11] Krebs et al. have suggested a mechanism for red kidney bean PAP (kbPAP) in which the substrate binds in a monodentate fashion to the M^{II} ion, while Fe^{III} provides a terminally bound OH^- as nucleophile at acidic pH (Scheme 1a).[5] By contrast, an alternative mechanism has been proposed for pig and sweet potato PAP in which the substrate forms a μ-1,3-phosphate complex, thus placing the μ-hydroxo bridge in an ideal position to act as the reaction-initiating nucleophile (Scheme 1b).[10,12,13] Recent studies have indicated that PAPs might employ a

*To whom correspondence should be addressed. E-mail: andrea.erxleben@nuigalway.ie. Phone: +353 91 492483. Fax: +353 91 525700.

(1) Mitić, N.; Smith, S. J.; Neves, A.; Guddat, L. W.; Gahan, L. R.; Schenk, G. *Chem. Rev.* **2006**, *106*, 3338–3363.
(2) Klabunde, T.; Krebs, B. *Struct. Bonding* (*Berlin*) **1997**, *89*, 177–198.
(3) Smith, S. J.; Casellato, A.; Hadler, K. S.; Mitić, N.; Riley, M. J.; Bortoluzzi, A. J.; Szpoganicz, B.; Schenk, G.; Neves, A.; Gahan, L. R. *J. Biol. Inorg. Chem.* **2007**, *12*(8), 1207–1220.
(4) Merkx, M.; Averill, B. A. *Biochemistry* **1998**, *37*, 8490–8497.
(5) Klabunde, T.; Sträter, N.; Fröhlich, R.; Witzel, H.; Krebs, B. *J. Mol. Biol.* **1996**, *259*, 737–748.
(6) Uppenberg, J.; Lindqvist, F.; Svensson, C.; Ek-Rylander, B.; Andersson, G. *J. Mol. Biol.* **1999**, *290*, 201–211.
(7) Lindqvist, Y.; Johansson, E.; Kaija, H.; Vihko, P.; Schneider, G. *J. Mol. Biol.* **1999**, *291*, 135–147.
(8) Guddat, L. W.; McAlpine, A. S.; Hume, D.; Hamilton, S.; de Jersey, J.; Martin, J. L. *Structure* **1999**, *7*, 757–767.
(9) Sträter, N.; Jasper, B.; Scholte, M.; Krebs, B.; Duff, A. P.; Langley, D. B.; Han, R.; Averill, B. A.; Freeman, H. C.; Guss, J. M. *J. Mol. Biol.* **2005**, *351*, 233–246.
(10) Schenk, G.; Gahan, L. R.; Carrington, L. E.; Mitić, N.; Valizadeh, M.; Hamilton, S. E.; de Jersey, J.; Guddat, L. W. *Proc. Natl. Acad. Sci. U.S. A.* **2005**, *102*, 273–278.
(11) Wilcox, D. E. *Chem. Rev.* **1996**, *96*, 2435–2458, and refs therein.
(12) Schenk, G.; Boutchard, C. L.; Carrington, L. E.; Noble, C. J.; Moubaraki, B.; Murray, K. S.; de Jersey, J.; Hanson, G. R.; Hamilton, S. *J. Biol. Chem.* **2001**, *276*, 19084–19088.
(13) Smoukov, S. K.; Quaroni, L.; Wang, X.; Doan, P. E.; Hoffman, B. M.; Que, L., Jr. *J. Am. Chem. Soc.* **2002**, *124*, 2595–2603.

© 2010 American Chemical Society
Published on Web 06/21/2010

Scheme 1. Proposed Mechanisms for Purple Acid Phosphatase Catalyzed Phosphate Ester Hydrolysis[a]

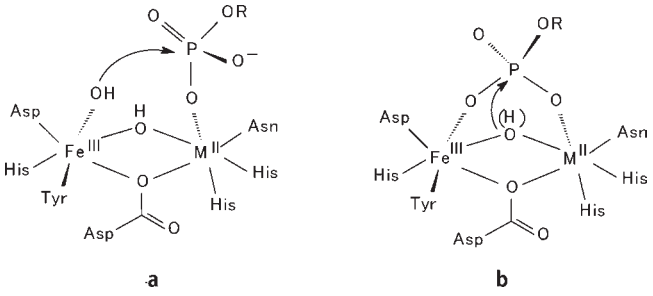

[a] In mechanism (a) coordination of the phosphate ester to the M^{II} ion is followed by nucleophilic attack by an Fe^{III}-bound hydroxide. In model (b) the bridging (hydr)oxo group acts as nucleophile.[5,10,12−14]

flexible mechanistic strategy ("one enzyme−two mechanisms" hypothesis), whereby the substrate coordination mode and the nature of the attacking nucleophile vary depending on the metal ion composition, the second coordination sphere, and the substrate itself.[3] Evidence has been obtained that uteroferrin PAP ($Fe^{III}Fe^{II}$ core) hydrolyzes phosphate diesters by the same mechanism proposed for kbPAP (Scheme 1a), while sweet potato PAP ($Fe^{III}Mn^{II}$ core) and the non-native $Ga^{III}Fe^{II}$, $Fe^{III}Ni^{II}$, and $Ga^{III}Zn^{II}$ forms of uteroferrin PAP employ a catalytic mechanism involving bridging substrate coordination and nucleophilic attack by a bridging hydroxo or oxo group (Scheme 1b).[3,14]

The catalytic activity of a metal ion is largely governed by its Lewis acidity. The stronger the Lewis activity, the stronger is the effect of the metal ion on substrate activation. On the other hand, an increase in the Lewis acidity of a metal ion results in a decrease of the nucleophilicity of a bound hydroxide. Fujii and co-workers studied the catalysis of the hydrolysis of phosphate triesters by Zn^{II} complexes and found an inverse correlation between the activity of the Zn complex and the pK_a value of zinc-coordinated water.[15] By contrast, an increase in the catalytic activity of macrocyclic Cu^{II} complexes with increasing pK_a value of $Cu-OH_2$ was reported by the same author for phosphodi- and -triester hydrolysis.[16] Kimura et al. compared the reactivity of the Zn complexes of 1,5,9-triazacyclododecane and 1,4,7,10-tetraazacyclododecane toward a phosphotri- and a phosphodiester and observed in both cases a decrease in reactivity with increasing pK_a of $Zn-OH_2$,[17] while Mancin and co-workers have recently reported a comprehensive study on a series of Zn complexes that revealed a positive correlation of the reaction rate of phosphate diester hydrolysis and the basicity of the Zn-bound nucleophile indicating that the efficiency of the nucleophile determines the intrinsic reactivity of the metal complex in this case.[18] Clearly, although metal-mediated phosphate ester hydrolysis has been studied for several decades, there is still a great need for further investigations.

We have synthesized a series of Ga^{III} complexes with the tripodal ligands shown in Figure 1 and investigated their reactivity toward the model phosphate diester bis(2,4-dinitrophenyl) phosphate (BDNPP). Coordination of the tetradentate ligands to octahedral Ga^{III} results in two vacant coordination sites, thus enabling a combination of substrate and nucleophile activation (Scheme 2).

Besides being a suitable mimic of Fe^{III}, Ga^{III} is characterized by a well-defined coordination chemistry and absence of a relevant redox chemistry, which allows for detailed reactivity studies without interference because of competing oxidative cleavage pathways. The aim of the study was 2-fold: First, we wanted to assess the effect of the ligand donor atoms on the Lewis acidity and on the catalytic properties of the M^{III} ion in PAP. In particular, the presence of the tyrosine residue in the active site of PAP prompted our interest. As mentioned above, the role of the phenolate group is believed to be the stabilization of the Fe^{III} ion. However, the donor strength of the phenolate ligand may also influence the catalytic activity. It is worthy of note that in hydrolytically active Zn and Mg enzymes, the metal ions are exclusively bound to imidazole, carboxylate, and amide donor groups. Second, as in the mechanism shown in Scheme 1b M^{III} participates in substrate activation and at the same time effects the nucleophilicity of the bridging hydroxide, we wanted to evaluate the relative importance of substrate activation and nucleophile efficiency.

Experimental Section

Materials and General Methods. Pyridine-2-carboxaldehyde, imino diacetate, diethyl iminodiacetate, glycine, 2-(chloromethyl)-pyridine hydrochloride, *p*-methoxyphenol, and $Ga(NO_3)_3$ were purchased from Aldrich and used as supplied. All of the other chemicals and solvents were of analytical or spectroscopic grade, purchased from commercial sources and used without further purification. Deuterated solvents were obtained from Apollo Scientific. BDNPP,[19] $[GaL^1(H_2O)_2]$,[20] H_3L^2,[21] H_3L^3,[22] H_2L^4,[23] H_3L^5,[24] and HL^6 [22] were prepared according to literature procedures. $[GaL^2(H_2O)_2]$ and $[GaL^5(H_2O)_2]$ were generated in situ by mixing equimolar amounts of $Ga(NO_3)_3$ and the respective ligand.

^1H and ^{13}C NMR spectra were recorded on Jeol ECX-400 and Varian 500 AR spectrometers and referenced to TSP ($\delta = 0.00$) and methanol ($\delta = 49.5$), respectively. The pD values of D_2O solutions were measured by use of a glass electrode and addition of a value of 0.4 to the pH meter reading.[25,26] The pD values were adjusted using concentrated DNO_3 and NaOD solutions.

UV/vis measurements were carried out using a Varian Cary 50 scan spectrophotometer coupled to a Grant thermostatted water circulation bath. FT-IR spectra were recorded on a PerkinElmer FT-IR spectrometer fitted with an ATR accessory. Elemental analyses (carbon, hydrogen, and nitrogen) were performed with a PerkinElmer 2400 Series II analyzer.

(14) Schenk, G.; Peralta, R. A.; Batista, S. C.; Bortoluzzi, A. J.; Szpoganicz, B.; Dick, A. K.; Herrald, P.; Hanson, G. R.; Szilagyi, R. K.; Riley, M. J.; Gahan, L. R.; Neves, A. *J. Biol. Inorg. Chem.* **2008**, *13*, 139–155.
(15) Itoh, T.; Fujii, Y.; Tada, T.; Yoshikawa, Y.; Hisada, H. *Bull. Chem. Soc. Jpn.* **1996**, *69*, 1265–1274.
(16) Itoh, T.; Hisada, H.; Usui, Y.; Fujii, Y. *Inorg. Chim. Acta* **1998**, *283*, 51–60.
(17) Koike, T.; Kimura, E. *J. Am. Chem. Soc.* **1991**, *113*, 8935–8941.
(18) Bonfá, L.; Gatos, M.; Mancin, F.; Tecilla, P.; Tonellato, U. *Inorg. Chem.* **2003**, *42*, 3943–3949.
(19) Bunton, C. A.; Farber, S. J. *J. Org. Chem.* **1969**, *34*, 767–772.
(20) Jarjayes, O.; Mortini, F.; du Moulinet d'Hardemare, A.; Philouze, C.; Serratrice, G. *Eur. J. Inorg. Chem.* **2005**, 4417–4424.
(21) Du Moulinet d'Hardemare, A.; Jarjayes, O.; Mortini, F. *Synth. Commun.* **2004**, *34*, 3975–3988.
(22) Chiu, Y.-H.; Canary, J. W. *Inorg. Chem.* **2003**, *42*, 5107–5116.
(23) McLendon, G.; Motekaitis, R. J.; Martell, A. E. *Inorg. Chem.* **1975**, *14*, 1993–1996.
(24) Ceccato, A. S.; Neves, A.; de Brito, M. A.; Drechsel, S. M.; Mangrich, A. S.; Werner, R.; Haase, W.; Bortoluzzi, A. J. *J. Chem. Soc., Dalton. Trans.* **2000**, 1573–1577.
(25) Glasoe, P. K.; Long, F. A. *J. Phys. Chem.* **1960**, *64*, 188–190.
(26) Mikkelsen, K.; Nielsen, S. O. *J. Phys. Chem.* **1960**, *64*, 632–637.

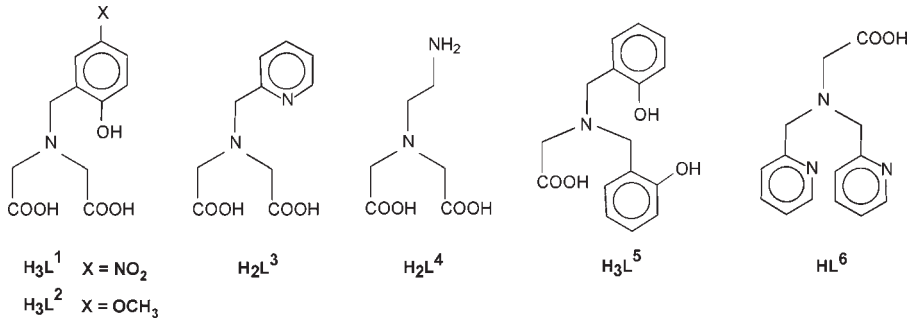

Figure 1. Ligands employed in this study.

Scheme 2. Substrate Activation and Nucleophilic Attack by a Ga-Bound Hydroxide

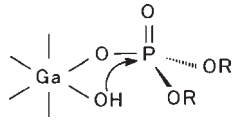

[GaL^3(μ-OH)]$_2$·4H$_2$O (3). Ga(NO$_3$)$_3$·8H$_2$O (2.92 g, 7.3 mmol) was dissolved in 50 mL of water. H$_2$L^3 (1.64 g, 7.3 mmol) was dissolved in 50 mL of water, and the two solutions were combined. The pH value was adjusted to 2.5 with 5 M NaOH. Slow evaporation of the solution over a period of 2 weeks yielded cubic crystals. Yield: 1.67 g (66%). ^{1}H NMR (D$_2$O): δ 8.72 (d, ^3J = 5.3 Hz, 1H), 8.29 (td, J = 7.8, 1.6 Hz, 1H), 7.82 (t, ^3J = 5.7 Hz, 1H), 7.77 (d, ^3J = 8.0 Hz, 1H), 4.76 (s, 2H), 3.92 (dd, ^2J = 17.6 Hz, 4H). ^{13}C NMR (D$_2$O): δ 174.7, 150.9, 145.9, 144.1, 127.1, 126.2, 62.6, 62.1. IR (cm^{-1}): 3222(br), 1666(m), 1622(s), 1445(w), 1378(s), 1340(m), 1309(m), 1269(w), 1153(w), 1104(w), 1027(w), 970(w), 911(m), 831(w), 773(m), 748(s), 728(m). Anal. Calcd (%) for C$_{20}$H$_{30}$Ga$_2$N$_4$O$_{14}$: C, 34.82; H, 4.38; N, 8.12; found: C, 34.90; H, 4.18; N, 8.54%.

[GaL^4(μ-OH)]$_2$·4H$_2$O (4). Ga(NO$_3$)$_3$·8H$_2$O (2.92 g, 7.3 mmol) was dissolved in water (50 mL) and added to an aqueous solution (50 mL) of H$_2$L^4 (1.28 g, 7.3 mmol). The pH value of the solution was adjusted to 5 with 5 M NaOH. Slow evaporation of the solution over a period of 2 weeks yielded small needles suitable for X-ray analysis. Yield: 980 mg (46%).^{1}H NMR (D$_2$O): δ 3.69 (m, 4H), 3.03 (s, br, 2H), 2.87 (s, br, 2H). ^{13}C NMR (D$_2$O): δ 176.3, 60.7, 58.23, 36.2. IR (cm^{-1}): 3225(br), 3091(w), 2987(w), 1608(s), 1393(m), 1301(m), 1210(w), 1175(w), 1100(w), 1070(m), 1053(m), 1000(w), 981(w), 917(m), 878(w), 789(w), 734(m). Anal. Calcd (%) for C$_{12}$H$_{30}$Ga$_2$N$_4$O$_{14}$: C, 24.27; H, 5.00; N, 9.49; found: C, 24.22; H, 4.41; N, 9.56%.

[Ga(HL^4)$_2$]Cl·2H$_2$O (4a). A solution of Ga(NO$_3$)$_3$·8H$_2$O (2.92 g, 7.3 mmol) in 50 mL of water was mixed with a solution of H$_2$L^4 (1.28 g, 7.3 mmol) in 50 mL of water. The pH value was brought to 3 with dilute HCl. **4a** crystallized as chloride salt with the chloride ions originating from HCl used to adjust the pH value. Yield: 1.12 g (62%). The colorless, cubic crystals of **4a** were insoluble in all common solvents. IR (cm^{-1}): 2913(br), 1638(s), 1523(w), 1381(s), 1364(s), 1348(m), 1315(m), 1251(w), 1176(w), 1107(w), 1051(m), 1000(m), 969(m), 942(m), 928(m), 907(s), 765(s). Anal. Calcd (%) for C$_{12}$H$_{26}$ClGaN$_4$O$_{10}$: C, 29.26; H, 5.33; N, 11.37; found: C, 28.53; H, 5.0; N, 11.30%.

[GaL^6(μ-OH)]$_2$(NO$_3$)$_2$·3H$_2$O (6). Ga(NO$_3$)$_3$·8H$_2$O (2.92 g, 7.3 mmol) was dissolved in 50 mL of water and added to a solution of HL^6 (1.87 g, 7.3 mmol) in water (50 mL). The pH value of the solution was adjusted to 2.5 using 5 M NaOH. Slow evaporation of the solution over a 2 week period yielded small needles of the dimer. Yield: 950 mg (30%). ^{1}H NMR (D$_2$O): δ 8.83 (d, ^3J = 5.24 Hz, 2H), 8.33 (td, J = 8.0, 1.6 Hz, 2H), 7.85 (m, 4H), 5.00 (d, ^2J = 16.48 Hz, 2H), 4.76 (d, ^2J = 16.48 Hz, 2H), 3.88 (s, 2H). ^{13}C NMR (D$_2$O): δ 174.6, 150.8, 145.9, 144.3, 127.2, 126.3, 61.8, 61.6. IR (cm^{-1}): 3092(br), 1611(s), 1469(w), 1450(w), 1369(s), 1336(s), 1306(s), 1269(m), 1160(w), 1098(m), 1053(w), 1031(m), 966(w), 908(m), 829(w), 767(s), 746(m). Anal. Calcd (%) for C$_{28}$H$_{36}$Ga$_2$N$_8$O$_{15}$: C, 38.92; H, 4.19; N, 12.97; found: C, 38.47; H, 4.07; N, 13.09%.

Potentiometric Titrations. Solutions of the Ga complexes **3**, **4**, **5**, and **6** (100 mL, 1 mM) in water (25 °C) were titrated with a standardized 0.1 M NaOH solution. The ionic strength was maintained at 0.1 M with KNO$_3$. pH values were measured with a Jenway 3510 pH meter fitted with a Refex Sensors Ltd. EC-1910-11 glass electrode. The program HYPERQUAD was used to calculate the deprotonation constants from the titration data.[27] Species diagrams were computed using a program based on the COMICS algorithm.[28]

Kinetic Measurements. The hydrolysis rate of BDNPP was measured by monitoring the increase in the visible absorbance at 400 nm because of the release of the 2,4-dinitrophenolate anion. Rate constants were obtained by the initial rate method (< 5% conversion). Concentrations of 2,4-dinitrophenolate were calculated from the extinction coefficient (12,100 M^{-1} cm^{-1}). Concentrations were corrected for the degree of ionization of 2,4-dinitrophenol at the respective pH value using pK_a (2,4-dinitrophenol) = 4.0.[29] In a typical experiment 15 μL of a freshly prepared BDNPP stock solution (10 mM in methanol) were added to a solution of the Ga complex (3 mL, 0.25−5 mM) at 37 °C. The metal complex solutions were buffered with 50 mM PIPBS (pH 4−5), MES (pH 5−6.7), HEPES (pH 6.8−8), EPPS (pH 7.5−8.5), and CHES (pH 8.5−9.5). The ionic strength was maintained at 0.1 M with NaClO$_4$. Hydrolysis rates have been corrected for the spontaneous hydrolysis of the substrate by following two identical parallel reactions except for the absence of metal complex in one of them. Kinetic runs were run in duplicate to give a reproducibility of ±15%. To determine the solvent deuterium isotope effect, analogous kinetic experiments were performed in H$_2$O and 99.9% D$_2$O. The correction pD = pH$_{measured}$ + 0.4 was applied to the pH meter readings.[25,26] k_D values for the reaction in D$_2$O were corrected for the uncatalyzed reaction in D$_2$O using the rate constant in water and the reported isotope effect for the spontaneous BDNPP cleavage.[19] Fitting of the kinetic data was carried out using a nonlinear least-squares program based on the NIHH23 algorithm.[30]

X-ray Analysis. Crystal data for **3**, **4**, **4a**, and **6** were collected at room temperature on an Oxford Diffraction Xcalibur CCD diffractometer using graphite-monochromated Mo−K$_\alpha$ radiation (λ = 0.71069 Å).[31] The structures were solved by direct

(27) Gans, P.; Sabatini, A.; Vacca, A. *Talanta* **1996**, *43*, 1739–1753.
(28) Ginzburg, G. *Talanta* **1977**, *23*, 149–152.
(29) Martell, A. E.; Smith, R. M. *Critical Stability Constants*; Plenum Press: New York, 1977.
(30) Fletcher, J. E.; Shrager, R. I. National Institute of Health, MD, U.S.A.
(31) *CrysAlisPro*, Version 1.171.33.31 (release 08−01−2009 CrysAlis171.NET); Oxford Diffraction Ltd.: Abingdon, U.K., 2009.

Table 1. Crystallographic Data for Compounds **3**–**6**

	3	**4**	**4a**	**6**
formula	$C_{20}H_{30}Ga_2N_4O_{14}$	$C_{12}H_{30}Ga_2N_4O_{14}$	$C_{12}H_{26}ClGaN_4O_{10}$	$C_{28}H_{36}Ga_2N_8O_{15}$
M_r	689.92	593.84	491.54	864.09
crystal color and habit	colorless block	colorless block	colorless plate	colorless cube
crystal size (mm)	0.20 × 0.20 × 0.10	0.30 × 0.30 × 0.20	0.20 × 0.15 × 0.05	0.30 × 0.20 × 0.15
crystal system	monoclinic	monoclinic	orthorhombic	monoclinic
space group	$P2_1/c$	$P2_1/c$	$Pccn$	$P2_1/c$
unit cell dimensions				
a [Å]	8.8492(3)	7.8500(7)	12.3409(7)	12.1675(4)
b [Å]	10.4470(4)	10.085(1)	16.974(1)	10.1530(3)
c [Å]	14.0948(5)	13.983(2)	9.6776(6)	14.3743(3)
β [deg]	90.216(2)	97.36(1)		94.478(2)
V [Å^3]	1303.02(8)	1097.9(2)	2027.3(2)	1770.33(9)
Z	2	2	4	2
D_{calc} (g cm^{-3})	1.758	1.796	1.610	1.621
μ(Mo K$_\alpha$) (mm^{-1})	2.146	2.530	1.546	1.603
F(000)	704	608	1016	884
2θ range (deg)	5.8−52.7	5.9−52.7	5.9−52.7	5.2−52.7
no. measd. reflections	8736	7619	14392	9049
no. unique reflections (R_{int})	2653 (2.9%)	2235 (2.5%)	2072 (9.5%)	3536 (2.2%)
no. of observed reflections	2087 ($I > 2\sigma(I)$)	1896 ($I > 2\sigma(I)$)	1470 ($I > 2\sigma(I)$)	2751 ($I > 2\sigma(I)$)
no. of parameters	181	145	129	238
Final R_1, wR_2 (observed reflections) [a]	R_1 = 3.0%, wR_2 = 8.4%	R_1 = 2.6%, wR_2 = 7.2%	R_1 = 5.6%, wR_2 = 15.7%	R_1 = 3.9%, wR_2 = 11.5%
Final R_1, wR_2 (all reflections) [a]	R_1 = 4.1%, wR_2 = 8.6%	R_1 = 3.1%, wR_2 = 7.3%	R_1 = 8.1%, wR_2 = 16.9%	R_1 = 5.4%, wR_2 = 12.0%
goodness-of-fit (observed reflections)	1.042	1.062	1.074	1.013

[a] $R_1 = \sum||F_o| - |F_c||/\sum|F_o|$; $wR_2 = [\sum w(F_o^2 - F_c^2)^2/\sum w(F_o^2)^2]^{1/2}$; $w^{-1} = \sigma^2(F_o^2) + (aP)^2$; $P = (F_o^2 + 2F_c^2)/3$.

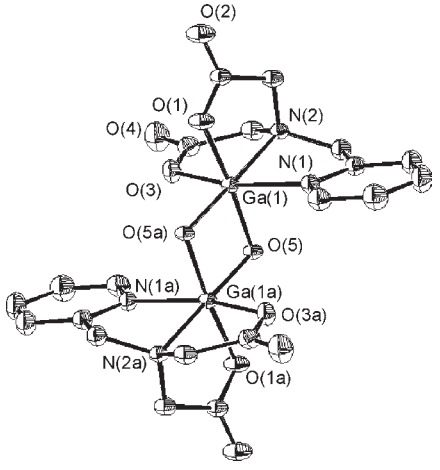

Figure 2. Molecular structure of [GaL^3(μ-OH)]$_2$·4H$_2$O (**3**) with the atom numbering scheme. Hydrogen atoms and water molecules of crystallization are omitted for clarity. Thermal ellipsoids are drawn at the 40% level.

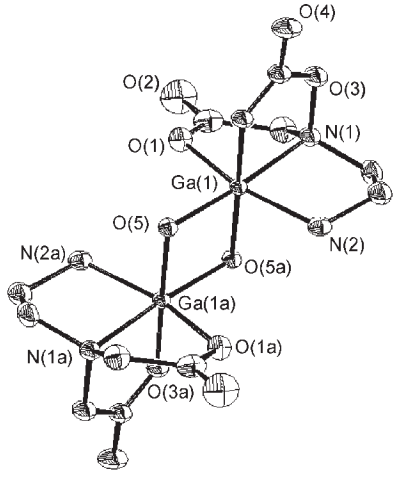

Figure 3. Molecular structure of [GaL^4(μ-OH)]$_2$·4H$_2$O (**4**) with the atom numbering scheme. Hydrogen atoms and water molecules of crystallization are omitted for clarity. Thermal ellipsoids are drawn at the 40% level.

methods and subsequent Fourier syntheses and refined by full-matrix least-squares on F^2 using SHELXS-97, SHELXL-97,[32] and Oscail.[33] The scattering factors were those given in the SHELXL program. Hydrogen atoms except those for the water molecules of crystallization were generated geometrically and refined as riding atoms with isotropic displacement factors equivalent to 1.2 times those of the atom to which they were attached (1.5 for methyl groups). Graphics were produced with ORTEX.[34]

Crystallographic data and details of refinement are reported in Table 1.

Density Functional Theory (DFT) Calculations. All DFT geometry optimizations were done in water at the B3LYP/6-31G* level using Spartan'08.[35]

Results

Synthesis and Characterization of the Ga^{III} Complexes. The mononuclear Ga complexes of H_3L^1 and H_3L^2, [GaL^1(H$_2$O)$_2$] (**1**) and [GaL^2(H$_2$O)$_2$] (**2**) have been reported in the literature.[20] Ga binds to the deprotonated phenolate oxygen, the amino nitrogen, and the two carboxylate groups of the tetradentate ligands, while two aqua ligands complete the octahedral coordination sphere.

(32) (a) Sheldrick, G. M. *SHELXS-97, Program for crystal structure solution*; University of Göttingen: Göttingen, Germany, 1997. (b) Sheldrick, G. M. *SHELXL-97, Program for crystal structure refinement*; University of Göttingen: Göttingen, Germany, 1997. (c) Sheldrick, G. M. *SHELXTL-PLUS* (*VMS*); Siemens Analytical X-ray Instruments, Inc.: Madison, WI, 1990.

(33) McArdle, P.; Gilligan, K.; Cunningham, D.; Dark, R.; Mahon, M. *CrystEngComm* **2004**, *6*, 303–309.

(34) McArdle, P. *ORTEX*, PC Windows version; *J. Appl. Crystallogr.* **1995**, *28*, 65.

(35) *Spartan'08*; Wavefunction, Inc.: Irvine, CA.

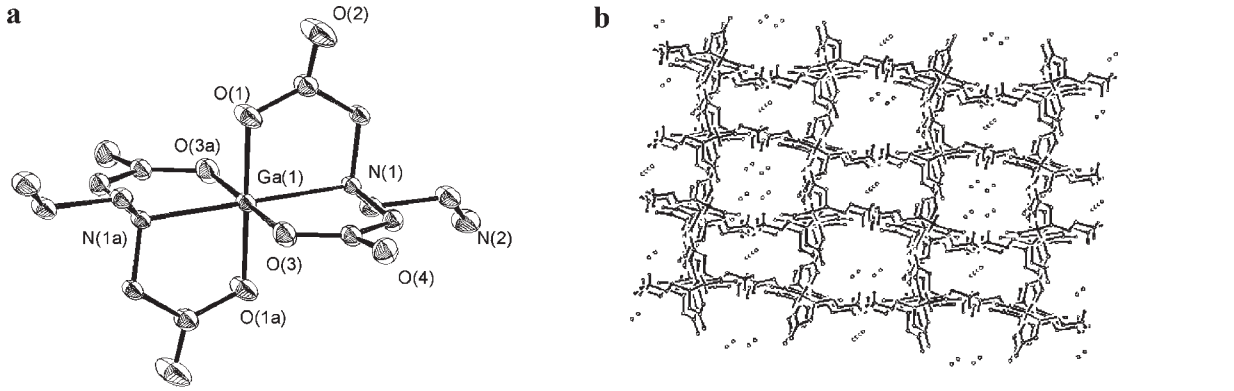

Figure 4. (a) View of the cation of $[Ga(HL^4)_2]Cl \cdot 2H_2O$ (**4a**) with the atom numbering scheme. Hydrogen atoms are omitted for clarity. Thermal ellipsoids are drawn at the 40% level. (b) Crystal packing of **4a**. The view is along the *b* axis.

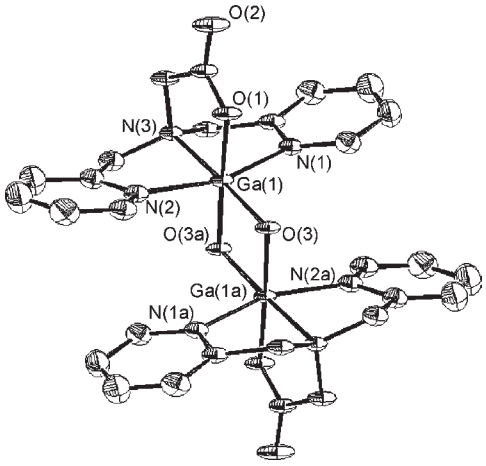

Figure 5. View of the cation of $[GaL^6(\mu\text{-}OH)]_2(NO_3)_2 \cdot 3H_2O$ (**6**) with the atom numbering scheme. Hydrogen atoms are omitted for clarity. Thermal ellipsoids are drawn at the 40% level.

Mixing the tripodal ligands H_2L^3, H_2L^4, and HL^6 with 1 equiv of $Ga(NO_3)_3$ at room temperature in the presence of base led to the isolation of the hydroxo-bridged dimers $[GaL^3(\mu\text{-}OH)]_2 \cdot 4H_2O$ (**3**), $[GaL^4(\mu\text{-}OH)]_2 \cdot 4H_2O$ (**4**), and $[GaL^6(\mu\text{-}OH)]_2(NO_3)_2 \cdot 3H_2O$ (**6**). By contrast, the mononuclear 2:1 complex $[Ga(HL^4)_2]Cl \cdot 2H_2O$ (**4a**) crystallized from more acidic solution in the presence of HCl. The Ga complex of H_3L^5 was characterized in solution by ^1H NMR spectroscopy (Supporting Information). It is postulated that the trianionic ligand forms a neutral complex of composition $[GaL^5(H_2O)_2]$ (**5**), analogously to **1** and **2**.

Figures 2−5 show the X-ray structures of complexes **3**−**6**, and selected bond lengths and angles are listed in Table 2. In the dimeric complexes **3**, **4**, and **6**, Ga is located in slightly distorted octahedral coordination environments formed by the respective tetradentate tripodal ligand and two bridging hydroxide groups. Ga···Ga distances lie in the range 2.951 to 2.982 Å. In all three structures, the hydroxo bridges are asymmetric with the bond to OH *trans* to the tertiary amino nitrogen being always the shorter one. Bond angles around the bridging oxygen range from 99.2 to 100.9°. Ga−N bond distances are longer for the tertiary amino nitrogen than for the primary amino group and pyridine nitrogen.

In the centrosymmetric 2:1 complex **4a**, Ga is situated on an inversion center (Figure 4a). The ligands coordinate through two carboxylate oxygens and the tertiary amino nitrogen, while the primary amino group is protonated and non-coordinating. Ga−O and Ga−N bond lengths fall in the typical range. In the crystal packing (Figure 4b), the cations form a channelled structure. Hydrogen bonds are observed between the ammonium groups, carboxylate oxygens, and methylene groups (N(2)···O(4) 2.842(2) Å, N(2)−H···O(4) 139°, $-x$, $1/2 + y$, $1/2 - z$; C(3)···O(2) 3.345(2) Å, C(3)−H(a)···O(2) 179°, $-1/2 + x$, $-y$, $1/2 - z$; C(3)···O(2) 3.243 Å, C(3)−H(b)···O(2) 169°, $1/2 - x$, y, $1/2 + z$). As evident from Figure 4b, two types of channels are present. The larger channels are filled with water molecules of crystallization, while the smaller ones accommodate the counterions. The water molecules of crystallization

Table 2. Selected Bond Lengths [Å] and Angles [deg] in Compounds **3**−**6**

		3	
Ga(1)−N(1)	2.084(2)	Ga(1)−N(2)	2.105(2)
Ga(1)−O(1)	1.975(2)	Ga(1)−O(3)	1.967(2)
Ga(1)−O(5)	1.982(2)	Ga(1)−O(5a)[a]	1.903(2)
Ga(1)···Ga(1a)[a]	2.9600(6)		
N(1)−Ga(1)−N(2)	78.21(9)	N(1)−Ga(1)−O(3)	159.69(9)
N(1)−Ga(1)−O(5)	90.14(8)	N(1)−Ga(1)−O(5a)[a]	102.25(9)
N(2)−Ga(1)−O(1)	84.92(8)	N(2)−Ga(1)−O(3)	81.75(8)
		4	
Ga(1)−N(1)	2.068(2)	Ga(1)−N(2)	2.029(2)
Ga(1)−O(1)	1.982(2)	Ga(1)−O(3)	1.983(2)
Ga(1)−O(5)	1.863(1)	Ga(1)−O(5a)[b]	2.002(2)
Ga(1)···Ga(1a)[b]	2.951(1)		
N(1)−Ga(1)−N(2)	84.20(8)	N(1)−Ga(1)−O(3)	83.45(7)
N(1)−Ga(1)−O(5)	174.52(7)	N(1)−Ga(1)−O(5a)[b]	100.21(7)
N(2)−Ga(1)−O(1)	162.45(8)	N(2)−Ga(1)−O(3)	91.11(8)
		4a	
Ga(1)−N(1)	2.086(3)	Ga(1)−O(1)	1.948(3)
Ga(1)−O(3)	1.948(3)		
N(1)−Ga(1)−O(1)	85.3(1)	N(1)−Ga(1)−O(3)	85.3(1)
O(1)−Ga(1)−O(3)	89.0(2)		
		6	
Ga(1)−N(1)	2.062(3)	Ga(1)−N(2)	2.061(3)
Ga(1)−N(3)	2.086(2)	Ga(1)−O(1)	1.976(2)
Ga(1)−O(3)	1.884(2)	Ga(1)−O(3a)[a]	1.982(2)
Ga(1)···Ga(1a)[a]	2.982(1)		
N(1)−Ga(1)−N(2)	159.2(1)	N(1)−Ga(1)−N(3)	80.2(1)
N(1)−Ga(1)−O(1)	85.8(1)	N(2)−Ga(1)−O(1)	89.0(1)
N(2)−Ga(1)−O(3)	101.1(1)	O(3)−Ga(1)−O(3a)[a]	79.12(9)

[a] $-1-x,1-y,1-z$. [b] $1-x,1-y,1-z$.

and the chloride anions form hydrogen bonds with the non-coordinating, protonated amino groups (N(2)···O(1w) 2.823(2) Å, $1/2 - x$, $1/2 - y$, z; N(2)···Cl 3.182(1) Å, $1/2 - x$, y, $1/2 + z$).

Solution Behavior. The stability of the 1:1 and hydroxo-bridged Ga complexes in aqueous solution has been studied by ^{1}H NMR spectroscopy. No dissociation into metal ion and free ligand takes place in the pD range 3−9.

pK_a values for the deprotonation of the aqua ligands in the mononuclear complexes **1** and **2** have been reported in the literature[20] and are listed in Table 3 along with the pK_a values determined for **3**−**6**. Dissolving the hydroxo-bridged Ga complexes **3**, **4**, and **6** at 1 mM concentration gave solutions with pH values between 5 and 6. Potentiometric titration over the pH intervals 5−9.5 (**3**), 6−9.5 (**4**), 5.5−10 (**5**), and 5−9 (**6**) revealed one titratable proton per Ga with a pK_a value of 7.38 (**3**), 7.78 (**4**), and 6.72 (**6**)

Table 3. Potentiometric and Kinetic Data for the Ga Complexes **1**−**6**

	pK_{a1}	pK_{a2}	pK_{a1}'[a]	pK_{a2}'[a]	K_{eq}[a] (M)	k (M^{-1} s^{-1})
1	5.54(2) [b]		5.43	8.59	0.541	2.12×10^{-2}
2	6.42(1) [b]		5.90	8.99	1.03×10^{-2}	3.05×10^{-2}
3		7.38(2) [c]	5.69	7.12	1.34×10^{-3}	3.61×10^{-3}
4		7.78(2) [c]	5.72	7.72	2.28×10^{-3}	3.86×10^{-3}
5	7.37(2) [c]	9.29(3) [c]	7.26	9.72	7.85	4.64×10^{-2}
6	6.72(3) [c]					

[a] Kinetic data. [b] Potentiometric data, ref 20. [c] Potentiometric data in the pH interval 5−9.5 (**3**), 6−9.5 (**4**), 5.5−10 (**5**), and 5−9 (**6**), this work.

(Supporting Information, Figure S2), thus suggesting the dissociation into monomeric aqua-hydroxo species, [GaL(H_2O)(OH)]. Species distribution curves for **3**−**6** are displayed in Supporting Information, Figure S3.

BDNPP Hydrolysis. Kinetic experiments have been carried out with the activated substrate bis(2,4-dinitrophenyl)phosphate (BDNPP). The hydrolysis reaction was monitored by following the increase in the visible absorbance at 400 nm because of the release of 2,4-dinitrophenolate. Pseudo-first-order rate constants k_{obs} for the formation of 2,4-dinitrophenolate were obtained from initial rates (< 5% conversion). Hydrolysis rates have been corrected for the spontaneous hydrolysis of the substrate. In the case of **6** long induction periods were observed which render the kinetic data difficult to interpret and for which we do not have a rational explanation at present. For **1**−**5** bell-shaped pH-rate profiles were obtained with maxima at pH 7.0 (**1**), 7.5 (**2**), 6.4 (**3**), 6.7 (**4**) and 8.5 (**5**) (Figure 6). The bell-shaped pH-rate profiles strongly suggest that the aqua-hydroxo forms of the complexes are the active species for hydrolyzing the phosphate diester.

The dependence of the rate of BDNPP hydrolysis on the concentration of **1**−**5** at the respective optimum pH is depicted in Figure 7. The cleavage rates initially increase linearly with increasing concentration of the metal complexes but gradually deviate from linearity because of the presence of hydroxo-bridged dimers in more concentrated solution.

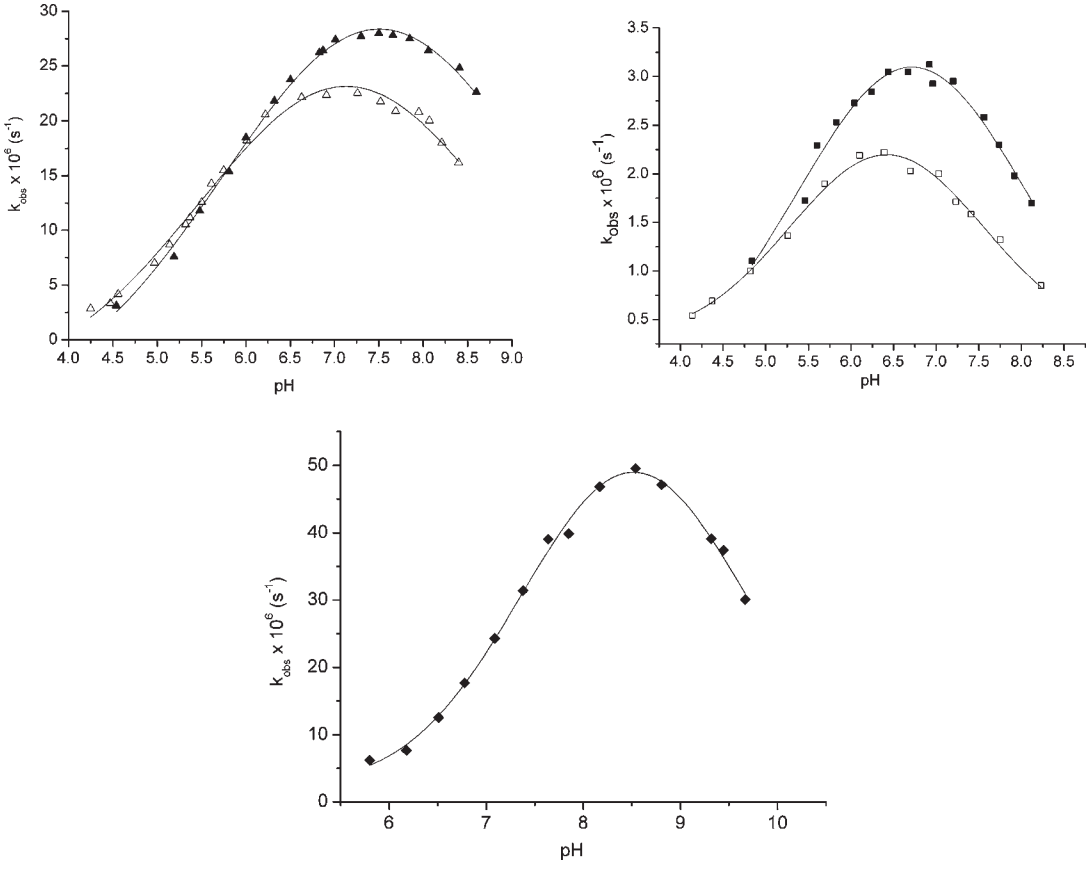

Figure 6. Rate-pH profiles for the cleavage of BDNPP (5×10^{-5} M) with 2 mM solutions of [$GaL^1(H_2O)(OH)]^-$ (△), [$GaL^2(H_2O)(OH)]^-$ (▲), [$GaL^3(H_2O)(OH)$] (□), [$GaL^4(H_2O)(OH)$] (■), and [$GaL^5(H_2O)(OH)]^-$ (♦) at 37 °C. [buffer] = 50 mM (buffer = PIPBS (pH 4−5), MES (pH 5−6.5), HEPES (pH 6.8−8), EPPS (pH 7.5−8.5), and CHES (pH 8.5−9.5); I = 0.1 M ($NaClO_4$).

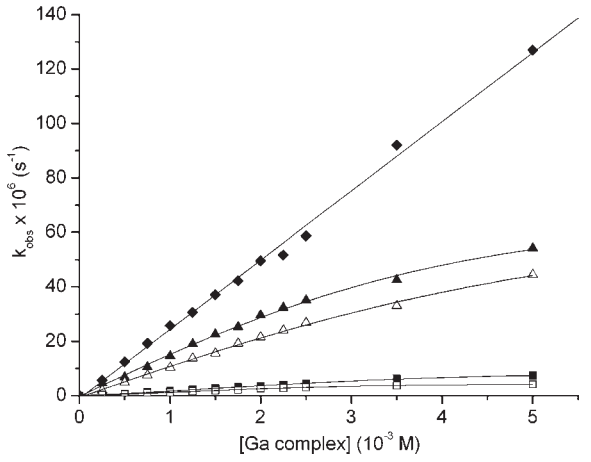

Figure 7. Dependence of the rate of cleavage of BDNPP (5×10^{-5} M) on the concentration of $[GaL^1(H_2O)(OH)]^-$ (△), $[GaL^2(H_2O)(OH)]^-$ (▲), $[GaL^3(H_2O)(OH)]$ (□), $[GaL^4(H_2O)(OH)]$ (■), and $[GaL^5(H_2O)(OH)]^-$ (♦) at 37 °C and the respective pH optimum, 50 mM buffer, $I = 0.1$ M ($NaClO_4$).

For the Ga complex mediated hydrolysis of BDNPP according to the mechanism displayed in Scheme 3, the following equations can be derived:

$$k_{obs} = A + k[Ga(H_2O)(OH)], \quad \text{where A is a constant} \tag{1}$$

$$[Ga]_t = 2[Ga_2L_2(\mu\text{-}OH)_2] + [GaL(H_2O)(OH)] + [GaL(H_2O)_2] + [GaL(OH)_2], \quad \text{where } [Ga]_t \text{ is the total Ga concentration} \tag{2}$$

$$[Ga]_t = \frac{2[GaL(H_2O)(OH)]^2}{K_{eq}} + [GaL(H_2O)(OH)]\left(1 + \frac{[H^+]}{K_{a1}} + \frac{K_{a2}}{[H^+]}\right) \tag{3}$$

Hence,

$$[GaL(H_2O)(OH)] = \frac{-\left(1 + \frac{[H^+]}{K_{a1}} + \frac{K_{a2}}{[H^+]}\right) \pm \sqrt{\left(1 + \frac{[H^+]}{K_{a1}} + \frac{K_{a2}}{[H^+]}\right)^2 + \frac{8}{K_{eq}}[Ga]_t}}{\frac{4}{K_{eq}}} \tag{4}$$

and

$$k_{obs} = A + k\frac{-\left(1 + \frac{[H^+]}{K_{a1}} + \frac{K_{a2}}{[H^+]}\right) \pm \sqrt{\left(1 + \frac{[H^+]}{K_{a1}} + \frac{K_{a2}}{[H^+]}\right)^2 + \frac{8}{K_{eq}}[Ga]_t}}{\frac{4}{K_{eq}}} \tag{5}$$

Fitting the kinetic data to eq 5 gave the K_{eq}, pK_a, and k values summarized in Table 3.

Scheme 3. Solution Equilibria of the Ga Complexes **1**− **5** and Phosphate Diester Hydrolysis

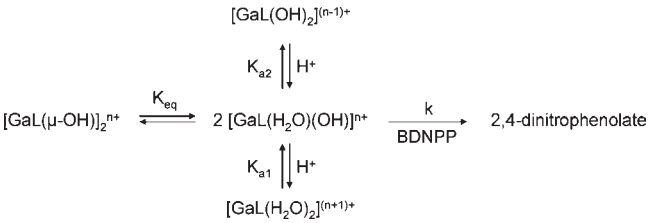

To gain more insight into the reaction mechanism, the solvent deuterium isotope effect k_H/k_D has been measured. The solvent deuterium isotope effect is the classical method for distinguishing between a nucleophilic and a general base mechanism. Generally, a k_H/k_D value ranging from 0.8 to 1.5 indicates a nucleophilic mechanism for phosphate ester hydrolysis, where no proton transfer is involved in the rate-determining step, while a k_H/k_D value greater than 2 supports a general base mechanism, where M−OH deprotonates an external water nucleophile.[36,37] k_H/k_D values for the five Ga complexes have been determined from pL-rate profiles (L = H, D) for the reactions in H_2O and D_2O (Supporting Information). Taking rate constants at corresponding pL values (pD = pH + 0.4) over the pL range studied gave k_H/k_D values of 1.09 ± 0.08 (**1**), 1.24 ± 0.13 (**2**), 0.95 ± 0.07 (**3**), 0.95 ± 0.03 (**4**), and 0.92 ± 0.06 (**5**).

Substrate binding to the aqua-hydroxo species was studied by ^{1}H NMR spectroscopy using the hydrolytically stable phosphate diester dimethyl phosphate (DMP). Upon addition of 1 equiv of DMP to a 2 mM solution of $[GaL^3(H_2O)(OH)]$ at pD 6.4, a new DMP doublet appeared 0.2 ppm downfield from the signal of free DMP (3.57 ppm). The presence of two signals indicates that the phosphate diester complex is kinetically inert on the NMR time-scale. No changes were observed in the ^{1}H NMR spectrum after longer reaction times. From the intensity ratio of the signals of bound and free DMP, the equilibrium constant for the anation of $[GaL^3(H_2O)(OH)]$ with DMP was estimated to be 6×10^1 M^{-1}. Similarly, equilibrium constants of ~7 and 2.5 M^{-1} were obtained for the coordination of DMP to the aqua-hydroxo species of **1** and **5**, respectively. Unfortunately, the determination of the equilibrium constants for substrate binding to **2** and **4** was hampered by severe overlap of DMP and ligand signals. Because of the limited solubility of the Ga complexes, ^{31}P NMR spectra could not be recorded.

DFT Calculations. The nucleophilicity of a metal-bound hydroxide depends on the metal−OH bond strength and therefore correlates with the M−OH bond length. DFT calculations have been carried out to determine the Ga−OH bond distances in the different aqua-hydroxo species. Geometry optimizations of $[GaL^1(H_2O)(OH)]^-$, $[GaL^2(H_2O)(OH)]^-$, $[GaL^3(H_2O)(OH)]$, $[GaL^4(H_2O)(OH)]$, and $[GaL^5(H_2O)(OH)]^-$ have been done in water at the B3LYP/6-31G level. Water and hydroxide groups have been placed trans to the tertiary amino nitrogen and trans to a carboxylate oxygen in the case of ligands HL^1−HL^4. On the basis of the X-ray structures of **1**, **3**, and **4**, it

(36) *Adv. Phys. Org. Chem.*; Gold, V., Ed.; Academic Press: New York, 1967.
(37) Cassano, A. G.; Anderson, V. E.; Harris, M. E. *J. Am. Chem. Soc.* **2002**, *124*, 10964–10965.

Table 4. Ga−OH Bond Distances (Å) in the Optimized Structures of the $[GaL(H_2O)(OH)]^{n-}$ Species

	OH trans to nitrogen, H_2O trans to oxygen	OH trans to oxygen, H_2O trans to nitrogen
$[GaL^1(H_2O)(OH)]^-$	1.865	1.875
$[GaL^2(H_2O)(OH)]^-$	1.872	1.885
$[GaL^3(H_2O)(OH)]$	1.841	1.854
$[GaL^4(H_2O)(OH)]$	1.859	1.873
$[GaL^5(H_2O)(OH)]^-$	1.907 [a]	1.896 [a]
	1.894 [b]	1.893 [b]

[a] Phenolate trans to phenolate. [b] Phenolate trans to carboxylate.

has been assumed that the phenolate oxygen, the amino nitrogen, and one carboxylate group coordinate meridionally in the solution structure of **1** and **2**, while in **3** and **4**, a carboxylate oxygen, the tertiary amino nitrogen, and pyridine/primary amino nitrogen occupy meridional coordination sites. As it is not clear, which of the two aqua ligands of the diaqua species has the lower pK_a value, both possible scenarios have been considered: (i) The hydroxo group is trans to the tertiary amino nitrogen, while the aqua ligand is trans to a carboxylate group and (ii) the hydroxo group is positioned trans to a carboxylate oxygen and the aqua ligand trans to the nitrogen. The former possibility is more likely. It is well-established that the relative acidity of coordinated water molecules is usually determined by the donor atom trans positioned to them. The weaker the metal−ligand interaction, the stronger is the metal-water interaction and the lower is the pK_a value. In the X-ray structures of the diaqua and hydroxo-bridged complexes **1**, **3**, and **4** the $Ga-N_{tert.am}$ bond is always longer than the Ga−O bonds suggesting that a water trans to nitrogen has the lower pK_a value. For **5**, four different scenarios have been considered: (i) the two phenolate groups trans to each other, the aqua ligand trans to the carboxylate group, and the hydroxo group trans to the nitrogen; (ii) the carboxylate group trans to a phenolate, the aqua ligand trans to the other phenolate oxygen, and the hydroxo group trans to nitrogen; (iii) the two phenolate groups trans to each other, the aqua ligand trans to the nitrogen, and the hydroxo group trans to the carboxylate; and (iv) the carboxylate group trans to a phenolate, the aqua ligand trans to the nitrogen, and the hydroxo group trans to a phenolate. The calculated Ga−OH bond distances for the aqua-hydroxo species of $H_3L^1-H_3L^5$ are listed in Table 4, and optimized structures are shown in Supporting Information, Figure S5. Ga−OH bond lengths vary from 1.841 to 1.907 Å, when the OH group is trans to nitrogen and from 1.854 to 1.896, when the OH group is trans to oxygen. In both cases the bond distance increases in the order $[GaL^3(H_2O)(OH)] < [GaL^4(H_2O)(OH)] < [GaL^1(H_2O)(OH)]^- < [GaL^2(H_2O)(OH)]^- < [GaL^5(H_2O)(OH)]^-$. That is, the longest Ga−OH bond is found, when Ga is bound to the two phenolate groups of H_3L^5.

Discussion

The bell-shaped pH-rate profiles with maximum k_{obs} values at pH values where the concentration of $[GaL(H_2O)(OH)]^{n+}$ is greatest indicate that the aqua-hydroxo species are the active species. The pH optimum shifts to higher pH values in the order **3** < **4** < **1** < **2** < **5**. The rate constant at the respective optimum pH value increases in the same order, with the difference between the rate acceleration provided by **3** and **5** being approximately 1 order of magnitude (Table 3). Kinetic data for the Ga complexes are consistent with the mechanism shown in Scheme 2, where the metal-bound hydroxide acts as the nucleophile on the coordinated substrate. The measured solvent deuterium isotope effect rules out a possible alternative mechanism, where the metal-bound hydroxide acts as a general base and deprotonates an incoming water nucleophile. k_H/k_D values measured for BDNPP hydrolysis in the presence of **1**−**5** range from 0.92 to 1.24, clearly suggesting nucleophilic rather than general base catalysis.

Generally, the acidity of coordinated water is considered a measure of the Lewis acidity of the metal ion. Kinetic pK_a values for the deprotonation of the first aqua ligand increase in the order **1** < **3** < **4** < **2** < **5**, while for the second pK_a the order is **3** < **4** < **1** < **2** < **5**. Although the pK_{a1} and pK_{a2} values do not offer a clear-cut picture of the order of increasing Lewis acidity of the central metal, it is clear that the Ga ions in the two most reactive complexes **2** and **5** possess the lowest Lewis acidities, thus providing the lowest substrate activation. DFT calculations showed that Ga−OH bond lengths in $[GaL(H_2O)(OH)]^{n-}$ become longer, that is, weaker, in the order **3** < **4** < **1** < **2** < **5**, suggesting the following trend in nucleophilicity of Ga-bound hydroxide: $[GaL^3(H_2O)(OH)] < [GaL^4(H_2O)(OH)] < [GaL^1(H_2O)(OH)]^- < [GaL^2(H_2O)(OH)]^- < [GaL^5(H_2O)(OH)]^-$. $[GaL^5(H_2O)(OH)]^-$ which has the strongest nucleophile, while its central metal ion is the weakest Lewis acid, is the most reactive catalyst. The correlation between nucleophilicity and catalytic activity indicates that the efficiency of the nucleophile prevails in determining the intrinsic reactivity of the Ga complexes. Apparently, the nucleophilicity of Ga−OH is more important than the Lewis acid activation of the phosphorus. A higher nucleophilicity also outweighs a lower substrate affinity, as the equilibrium constant for phosphate diester binding is 1 order of magnitude larger for complex **3** than for **1**, yet **1** is the better catalyst. It is worthy of note that $[GaL^1(H_2O)(OH)]^-$, $[GaL^2(H_2O)(OH)]^-$, and $[GaL^5(H_2O)(OH)]^-$ are reactive catalysts notwithstanding their negative charge which should render binding of anionic phosphate diesters difficult.

Equilibrium constants K_{eq} for the equilibrium between aqua-hydroxo species and (hydrolytically inactive) hydroxo-bridged dimers have been obtained from the kinetic data and increase in the order **5** < **1** < **2** < **4** < **3**. As expected, the anionic aqua-hydroxo species show a lower tendency to dimerization than the neutral ones.

It is well-known that the donor properties of the ligand influence the metal-water and metal-hydroxide interaction. The stronger the metal ligand bond, the weaker is the metal-water/hydroxide interaction in aqua and hydroxo species. As evident from the kinetic data for the different Ga complexes, the presence of a phenolate donor site apparently confers higher catalytic activity than does a neutral nitrogen donor site. In the X-ray structures of the mono- and dinuclear complexes **1**, **3**, and **4** with the ligands providing $N_{tert.am}(COO)_2O_{Phe}$, $N_{tert.am}(COO)_2N_{py}$, and $N_{tert.am}(COO)_2N_{prim.am}$ donor sets, the $Ga-O_{Phe}$ bond distance (1.884(2) Å[20]) is significantly shorter than the $Ga-N_{py}$ (2.084(2) Å) and the $Ga-N_{prim.am}$ (2.029(2) Å) bond length. This suggests that the presence of strongly electron-donating phenolate groups in the coordination sphere of Ga weakens the metal-hydroxide bond, thus

giving rise to an enhanced nucleophilicity and corroborating the results from the DFT calculations for the aqua-hydroxo species. Notably, in the most active catalyst, Ga is bound to two phenolate oxygens. The effect of the electron-donating properties of the ligand on the reactivity is further manifested, when the reactivities of **1** and **2** are compared. In both complexes, Ga is surrounded by a $N(COO)_2O_{Phe}$ donor set. The ligand in **2** whose phenolate group bears a strongly electron-donating methoxy group leads to a higher activity than the ligand in **1** having an electron-withdrawing substituent. While the catalytic activity follows the trend in Ga−OH bond strength, the correlation between reactivity and basicity of the nucleophile is less clear. The kinetic pK_a values for the deprotonation of the first aqua ligand increase in the order **1** < **3** ≈ **4** < **2** < **5**, whereas the order of activity is **3** < **4** < **1** < **2** < **5**. It should also be noted that there is no proportional correlation between the difference in pK_a and the difference in the rate constant. As the nucleophilicity is generally related to the basicity, this suggests that although the nucleophilicity is the key factor in determining the catalytic activity, other factors, like, for example, steric factors and/or substrate activation also contribute.

The observation that the presence of phenolate donor groups has a positive effect on the catalytic activity is relevant with regard to the tyrosinate ligand in the coordination sphere of the M^{III} ion in PAP. Our model studies and DFT calculations showed that upon replacing a pyridine nitrogen (which can be considered a mimic of the imidazole residue of histidine) by phenolate, the Ga−OH bond length increases by about 0.03 Å leading to an almost 10-fold increase in rate enhancement. The present results suggest that besides stabilizing the +III oxidation state, the tyrosinate ligand in PAP contributes to the generation of a strong nucleophile. When the mechanism depicted in Scheme 1b is operative, the influence of the trivalent ion on the bridging μ-OH group (nucleophile activation) seems to be more important than the effect of the M^{III} ion on the coordinated phosphate ester (substrate activation).

Acknowledgment. Financial support from Science Foundation Ireland (Stokes Lectureship to A.E.) is gratefully acknowledged. F.C. thanks NUI Galway for a College Fellowship.

Supporting Information Available: X-ray crystallographic data of complexes **3**, **4**, **4a**, and **6** in CIF format; ^{1}H NMR spectrum of $[GaL^5(H_2O)_2]$ generated in situ; potentiometric titration curves for **3**, **4**, **5**, and **6**; species distribution diagrams for **3**−**5** obtained from kinetic data; determination of k_H/k_D from pL-rate profiles; optimized structures of the aqua hydroxo species $[GaL^1(H_2O)(OH)]^-$, $[GaL^2(H_2O)(OH)]^-$, $[GaL^3(H_2O)(OH)]$, $[GaL^4(H_2O)(OH)]$, and $[GaL^5(H_2O)(OH)]^-$. This material is available free of charge via the Internet at http://pubs.acs.org.